BIFURCATIONS OF THE TWO-FREQUENCY FERMI MAPPING

by

J. E. Howard, M. A. Lieberman and A. J. Lichtenberg

Memorandum No. UCB/ERL M81/56

29 July 1981

ELECTRONICS RESEARCH LABORATORY

College of Engineering
University of California, Berkeley
94720

BIFURCATIONS OF THE TWO-FREQUENCY FERMI MAPPING

J.E. Howard, M.A. Lieberman and A.J. Lichtenberg
Department of Electrical Engineering and Computer Sciences
and the Electronics Research Laboratory
University of California, Berkeley, California 94720

Research sponsored by the Office of Naval Research Contract N00014-79-C-0674
and the Department of Energy Contract DE-ATOE-76-ET53059.

1. Introduction

In a recent paper [1] we investigated the effect of two driving frequencies on the stability properties of the Fermi map [2-4]. In particular, we found that by dividing the input power between two frequency components, the adiabatic limit to stochastic heating could be more than doubled. The purpose of this report is to provide supplementary material on the structure of the primary island chains discussed in the first paper.

We begin by deriving an appropriate island width for use in overlap criteria by means of an approximate averaged Hamiltonian. Next we classify the possible types of bifurcations that can occur as an island chain metamorphoses from one symmetry to another. The three possible classes of bifurcations are then related to the shape of the effective potential occurring in the averaged Hamiltonian. Analytic expressions are obtained for the critical values of the amplitude ratio and angular locations of the bifurcation sequence in a number of interesting cases, and compared with numerical solutions of the mapping equations. Explicit formulas are derived for the island width in the three simplest cases, with frequency ratios 2/1, 3/2, and 3/1.

2. Derivation of Averaged Hamiltonian

The symmetrized two-frequency Fermi mapping is [1]

$$u_{n+1} = u_n + \frac{\sin s\phi_n + \mu \sin r\phi_n}{\sqrt{1+\mu^2}} \tag{1}$$

$$\phi_{n+1} = \phi_n + \frac{2\pi M_{eff}}{u_{n+1}}, \tag{2}$$

where u_n and ϕ_n are the velocity and phase after the nth collision, μ in the amplitude ratio, r and s are coprime integers, and M_{eff} is a constant. This mapping is area preserving and periodic in ϕ

with period 2π. Equations (1) and (2) are derivable from the exact Hamiltonian

$$H = 2\pi M_{eff} \ln u - \frac{1}{\sqrt{1+\mu^2}} \left[\frac{1}{s} \cos s\phi + \frac{\mu}{r} \cos r\phi\right] \sum_{\ell=-\infty}^{\infty} e^{2\pi i \ell n}, \quad (3)$$

where the summation arises from the Fourier-expansion of a train of delta functions.

Introducing slow variables $\hat{u} = u - u_0$ and $\hat{\phi} = \phi - \phi_0$, where u_0 and ϕ_0 are the fixed point coordinates, and linearizing the first term in (3), we obtain the averaged Hamiltonian [1]

$$\hat{H} = \frac{1}{2} G\hat{u}^2 - \frac{1}{\sqrt{1+\mu^2}} \left(\frac{1}{s} \cos s\hat{\phi} + \frac{\mu}{r} \cos r\hat{\phi}\right), \quad (4)$$

where

$$G \equiv \frac{2\pi M_{eff}}{u_0^2} . \quad (5)$$

For given $\hat{H}$ and μ, (4) gives level curves $\hat{u} = \hat{u}(\hat{\phi})$ which closely approximate the mapping (1-2) in the vicinity of an island chain whose fixed points are common to both the r-fold and s-fold resonances. These common fixed points (u_{0k}, ϕ_0) are given by

$$\sin s\phi_0 + \mu \sin r\phi_0 = 0 \quad (6)$$

$$u_{0k} = \frac{M_{eff}}{k} , \quad k = 1,2,3,\ldots . \quad (7)$$

It is instructive to view (4) as representing the one-dimensional motion of a particle of effective mass G in the effective potential

$$V(\hat{\phi}) = - \frac{1}{\sqrt{1+\mu^2}} \left(\frac{1}{s} \cos s\hat{\phi} + \frac{\mu}{r} \cos r\hat{\phi}\right). \quad (8)$$

As μ increases from 0 to ∞, the shape of $V(\phi)$ changes from s-fold to r-fold symmetry. These changes are intimately related to topological changes in the level curves, so that some of the fixed points must bifurcate at certain critical values of μ. The model Hamiltonian (4)

is particularly interesting to study as it occurs in other contexts, such as particle trapping in two waves [5]. In section 3 we employ the language and tools of elementary catastrophe theory [6-7] to classify the possible bifurcations and calculate them in detail for several interesting cases.

2. Island Width

We have seen that as μ varies, radical topological changes in the island structure make it impossible to define an island width at an arbitrary position ϕ. However, the fixed point at $\phi = 0$ is always elliptic, and this fact provides us with a well-defined island width for use in overlap criteria. Figure 1 shows a typical separatrix, given by (4),

$$\frac{1}{2} G \hat{u}^2 = E_{sep} + \frac{1}{\sqrt{1+\mu^2}} \left(\frac{1}{s} \cos s\phi + \frac{\mu}{r} \cos r\phi\right), \tag{9}$$

where

$$E_{sep} = \frac{-1}{\sqrt{1+\mu^2}} \left(\frac{1}{s} \cos s\phi_c + \frac{\mu}{r} \cos r\phi_c\right) \tag{10}$$

with ϕ_c the crossing phase closest to $\phi = 0$. In general ϕ_c must be extracted numerically from the several solutions of (6) for each μ. The maximum island width $\Delta \equiv \hat{u}_{max}$ is then given by putting $\phi = 0$ in (9);

$$\Delta^2 = \frac{4}{G\sqrt{1+\mu^2}} \left[\frac{1}{s} \sin^2\left(\frac{s\phi_c}{2}\right) + \frac{\mu}{r} \sin^2\left(\frac{r\phi_c}{2}\right)\right] . \tag{11}$$

The widths for $\mu = 0$ and ∞ are given by setting $s\phi_c$ and $r\phi_c = \pi$, respectively, in (11), so that

$$\frac{\Delta(0)}{\Delta(\infty)} = \sqrt{\frac{r}{s}} . \tag{11a}$$

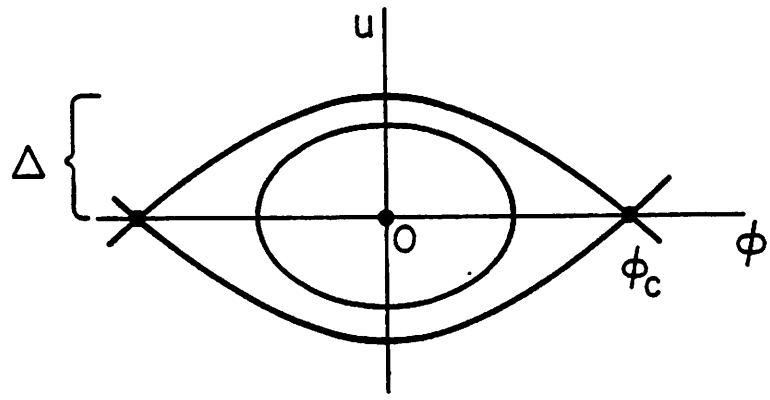

Fig. 1. Central island separatrix showing island width $\Delta = u_{max}$ and crossing phase ϕ_c.

The behavior of $\Delta(\mu)$ in between these limits may be understood by examining the derivative,

$$\frac{\partial \Delta^2}{\partial \mu} = \frac{4}{(1+\mu^2)^{3/2}} \left[\frac{1}{r} \sin^2\left(\frac{r\phi_c}{2}\right) - \frac{\mu}{s} \sin^2\left(\frac{s\phi_c}{2}\right)\right]. \tag{11b}$$

For $\mu << 1$, $\Delta^2/\partial\mu$ may be positive or zero depending on ϕ_c, but $\Delta(\mu)$ is monotonically decreasing over most of the range of u, where the second term of (11b) dominates. Generally $\Delta(\mu)$ has a gentle maximum near $\mu = 0.5$, varying by only a few percent over the range of interest. In the important case $r = s + 1$, $\Delta(\mu)$ varies only slightly over the entire range, and we may take $\Delta(\mu) \approx \Delta(0)$. In section 4 we obtain explicit expressions for $\Delta(\mu)$ for r/s = 2/1, 3/2 and 3/1.

3. Classification of Bifurcations

Straightforward linear stability analysis [1] of the mapping (1-2) shows that bifurcations occur at critical μ^* and ϕ_0^* given by the simultaneous solutions of

$$\sin s\phi_0 + \mu \sin r\phi_0 = 0 \tag{12}$$

$$s \cos s\phi_0 + \mu r \cos s\phi_0 = 0. \tag{13}$$

These equations admit a simple geometrical interpretation if we observe that they are equivalent to $V'(\phi_0) = V''(\phi_0) = 0$. That is, eq. (12), which locates the fixed points, has a double root at $\phi_0 = \phi_0^*$. Bifurcations occur when fixed points merge. Thus, the averaged Hamiltonian (4) with the effective potential (8) retains the basic topological features of the exact mapping in the neighborhood of the common fixed points. For our purposes we can therefore drop the distinction between local averaged and the exact variables and write (u,ϕ) for $(\hat{u},\hat{\phi})$ in applying the results of section 2. We now examine

CLASSIFICATION OF BIFURCATIONS

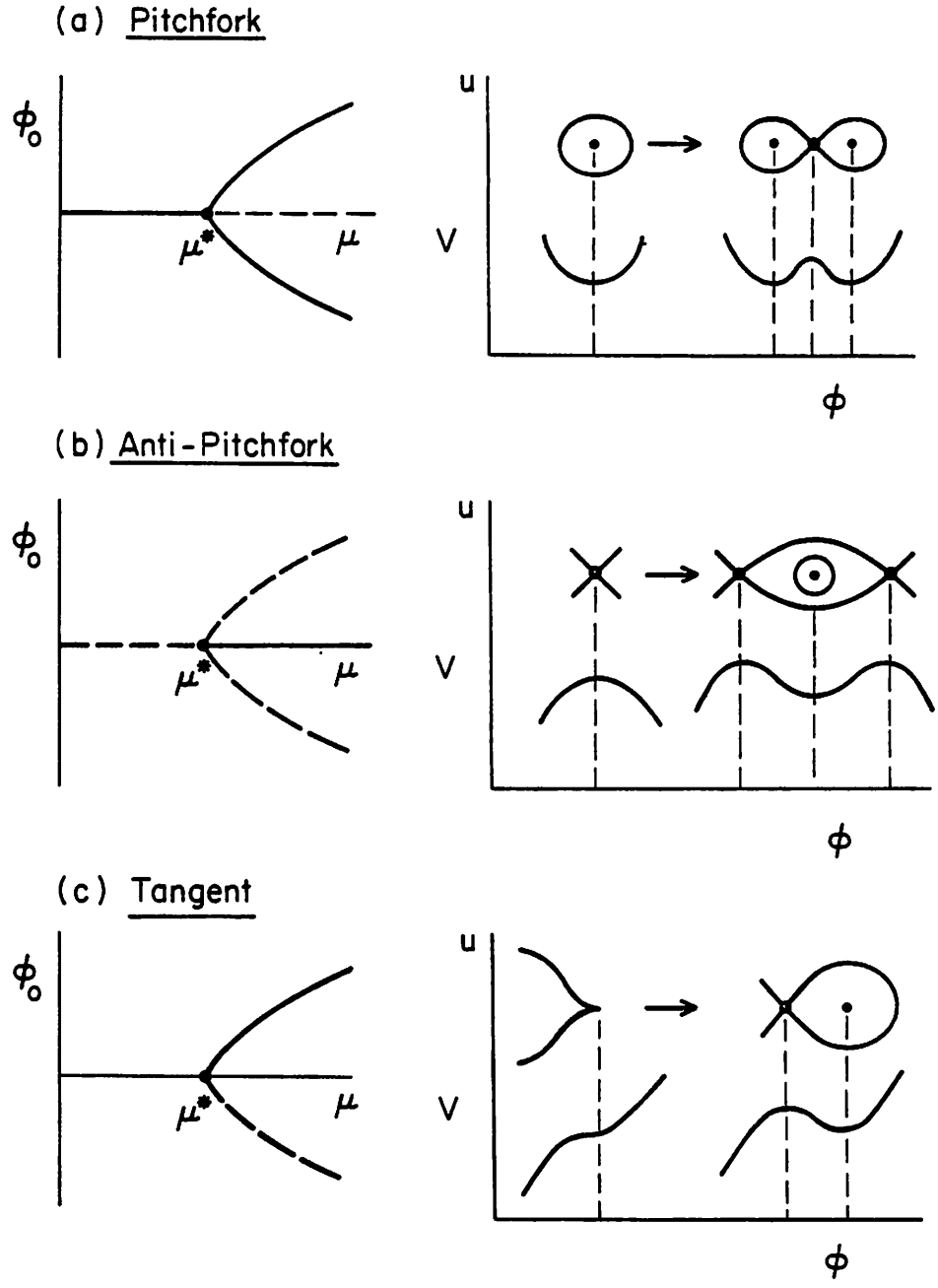

Fig. 2. Bifurcation types for a general periodic potential: (a) tangent bifurcation, for which $V(\phi)$ has an inflection point; (b) pitchfork bifurcation ($V''' = 0$, $V^{iv} > 0$); (c) anti-pitchfork bifurcation ($V''' = 0$, $V^{iv} < 0$).

the possible types of bifurcation for a general periodic potential $V(\phi)$, based on some notions of elementary catastrophe theory [6].

(a) Tangent Bifurcation (Pair Creation) ($V_0''' \neq 0$)

When $V_0''' \neq 0$, $V(\phi)$ has an inflection point at ϕ_0^* for the critical value μ^*. As μ is increased further, $V(\phi)$ develops a min-max pair, giving rise to a stable-unstable pair of fixed points, as illustrated in Fig. 2(a).

(b) Pitchfork Bifurcation ($V_0''' = 0$, $V_0^{iv} > 0$)

When $V_0''' = 0$, the function $V(\phi_0)$ has a third order critical point at ϕ_0^*. This kind of bifurcation requires symmetry with respect to $\phi_0 = \pi$ for the Fermi map. As μ is increased beyond μ^*, $V(\phi)$ develops a dimple in the center of a broad minimum, and the original elliptic fixed point goes unstable, issuing forth two new stable fixed points to either side, as shown in Fig. 2(b).

(c) Anti-Pitchfork Bifurcation ($V_0''' = 0$, $V_0^{iv} < 0$)

When $V_0^{iv} < 0$, $V(\phi)$ has a broad maximum at ϕ_0^*, which develops a local minimum as μ increases beyond μ^*. The original hyperbolic fixed point then stabilizes, escorted by two new hyperbolic fixed points, as depicted in Fig. 2(c). Again, by symmetry this can only occur at $\phi_0 = \pi$ for the Fermi map.

4. Closed Form Solutions

In general, eqs. (12) and (13) must be solved numerically. However, algebraic solutions may be obtained for $s < r \leq 5$ and for the cases $r = s + 1$ and $r = s + 2$. Detailed study of these tractable cases then provides us with clues concerning the order and manner in which fixed points bifurcate in general.

Let us begin by examining the stability of the obvious fixed points at $\phi_0 = 0$ and $\pm\pi$. Setting $\phi = 0$ in Eq. (13) immediately shows that this (elliptic) fixed point never bifurcates for positive μ. On the other hand, the $\phi_0 = \pm\pi$ points (actually the same point modulo 2π) bifurcate at $\mu^* = s/r$ whenever $r - s$ is odd. In particular, if $r - s = 1$, this is the only bifurcation, giving birth to two new fixed points, exactly the required number to change from s-fold to (s+1)-fold symmetry.

Another broad class of bifurcations is revealed by setting $\phi_0 = \pm \frac{\pi}{2}$ in Eqs. (12) and (13). Taking $r = s + 2m$ ($m = 1,2,\ldots$) then satisfies Eq. (13), since r and s must be odd in order to be coprime. Equation (12) becomes $1+\mu \cos m\pi = 0$, which is satisfied by $\mu = 1$ and m odd. Thus, a pair of tangent bifurcations always occurs at $\phi_0^* = \pm \frac{\pi}{2}$ when $\mu^* = 1$ for $r = s + 2, s + 6,\ldots$ Again, when $r - s = 2$ these are the only bifurcations as μ increases from 0 to ∞.

When $s < r \leq 5$, complete algebraic solutions of (12) and (13) may be obtained by means of the factorization

$$\sin n\phi = \sin\phi \, P_{n-1}(\cos\phi), \tag{14}$$

where P_{n-1} is a polynomial of degree n-1. Thus, (12) becomes

$$P_{s-1}(x) + \mu P_{r-1}(x) = 0, \tag{15}$$

where $x \equiv \cos\phi$. The critical values of μ are then usually given by the vanishing of the discriminant of (15). We now consider the various cases for which this procedure is possible. The first three cases are treated in detail as paradigms for the three varieties of bifurcation.

4.1 $\boxed{r/s = 2/1}$

In this the simplest combination of frequencies, the $\mu = 0$ fixed points lie at $\phi_0 = 0$ and π. Since $r = s + 1$, a single bifurcation takes place at $\phi_0^* = \pi$. Formally, (15) gives

$$\sin\phi_0(1+2\mu\cos\phi_0) = 0, \tag{16}$$

whose solutions are $\phi_0 = 0, \pi$ and

$$\cos\phi_0 = -\frac{1}{2\mu} \ . \tag{17}$$

As ϕ_0 is complex for $\mu < 1/2$, $\mu^* = 1/2$ is the critical value, for which $\phi_0^* = \pi$. At this point $V_0''' = 0$ and $V_0^{iv} = -3$, indicating an anti-pitchfork bifurcation. Figure 3 shows the level curves and effective potentials calculated from the averaged Hamiltonian (4) for several values of μ. These may be seen to compare well with the exact mappings shown in Fig. 4, most clearly for the chain at $u = 33.33$.

The separatrix is particularly easy to calculate in this case; from (9), (10) and (17) we find

$$\sqrt{1+\mu^2}Gu^2 = \begin{cases} 4\cos^2\frac{\phi}{2}\,(1-2\mu\sin^2\frac{\phi}{2}), & \mu \leq \mu^* \\ \frac{1}{2\mu} + 2\cos\phi(1+\mu\cos\phi), & \mu \geq \mu^* \end{cases} \tag{18}$$

Thus, $u \sim \pm\cos\phi$ when $\mu = \mu^* = 1/2$. Putting $\phi = 0$ in (18) we obtain the central island width as a function of μ, which is plotted along with the widths for $r/s = 3/2$ and $3/1$ in Fig. 5. Note that Δ decreases monotonically and that $\Delta(0) = \sqrt{2}\,\Delta(\infty)$, as predicted by (11a). In studying the increase in the adiabatic barrier to stochastic heating we are primarily interested in the parameter range $0 \leq \mu \lesssim 1$, for which the characteristic overlapping of neighboring islands occurs. The curves in Fig. 5 show that even in the worst case $r/s = 1/2$,

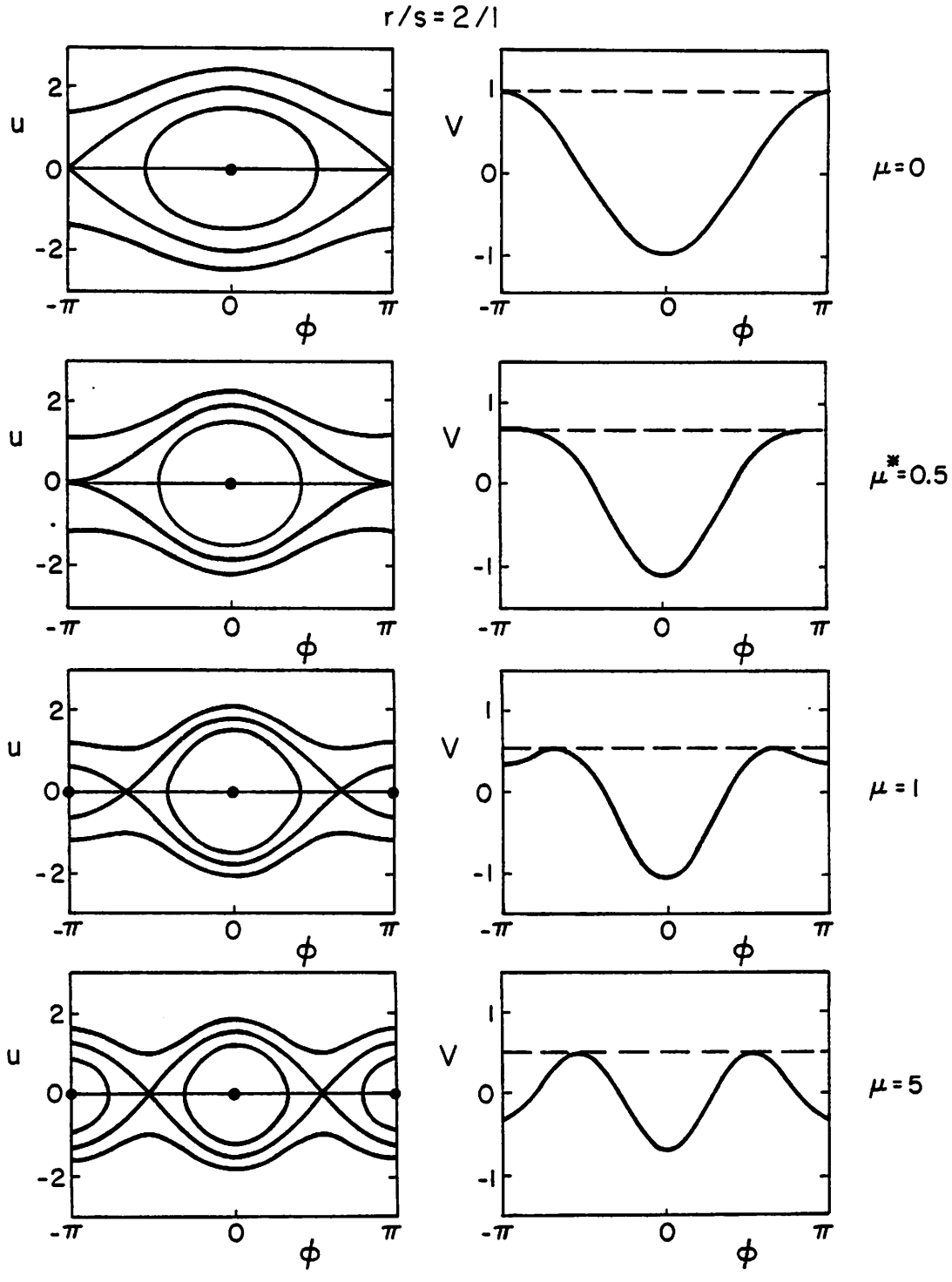

Fig. 3. Level curves and effective potential for r/s = 2/1. An anti-pitchfork bifurcation occurs at $\phi = \pi$ when $\mu = 0.5$. The dashed lines are the energy levels of the separatrix.

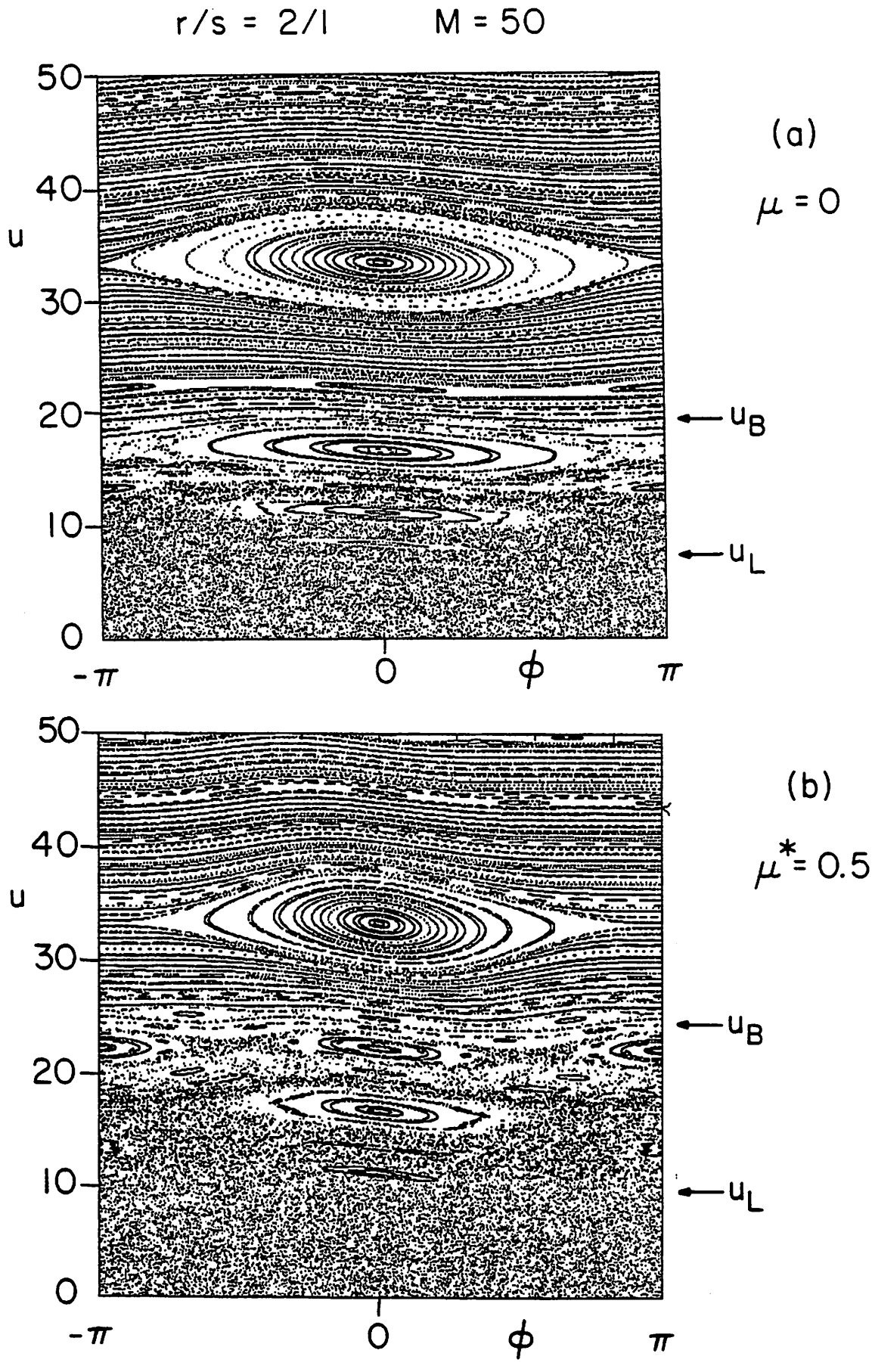

Fig. 4. Computer-produced mappings for r/s = 2/1, M = 50. Note the increase in the adiabatic barrier u_B and linear stability limit u_L with increasing μ.

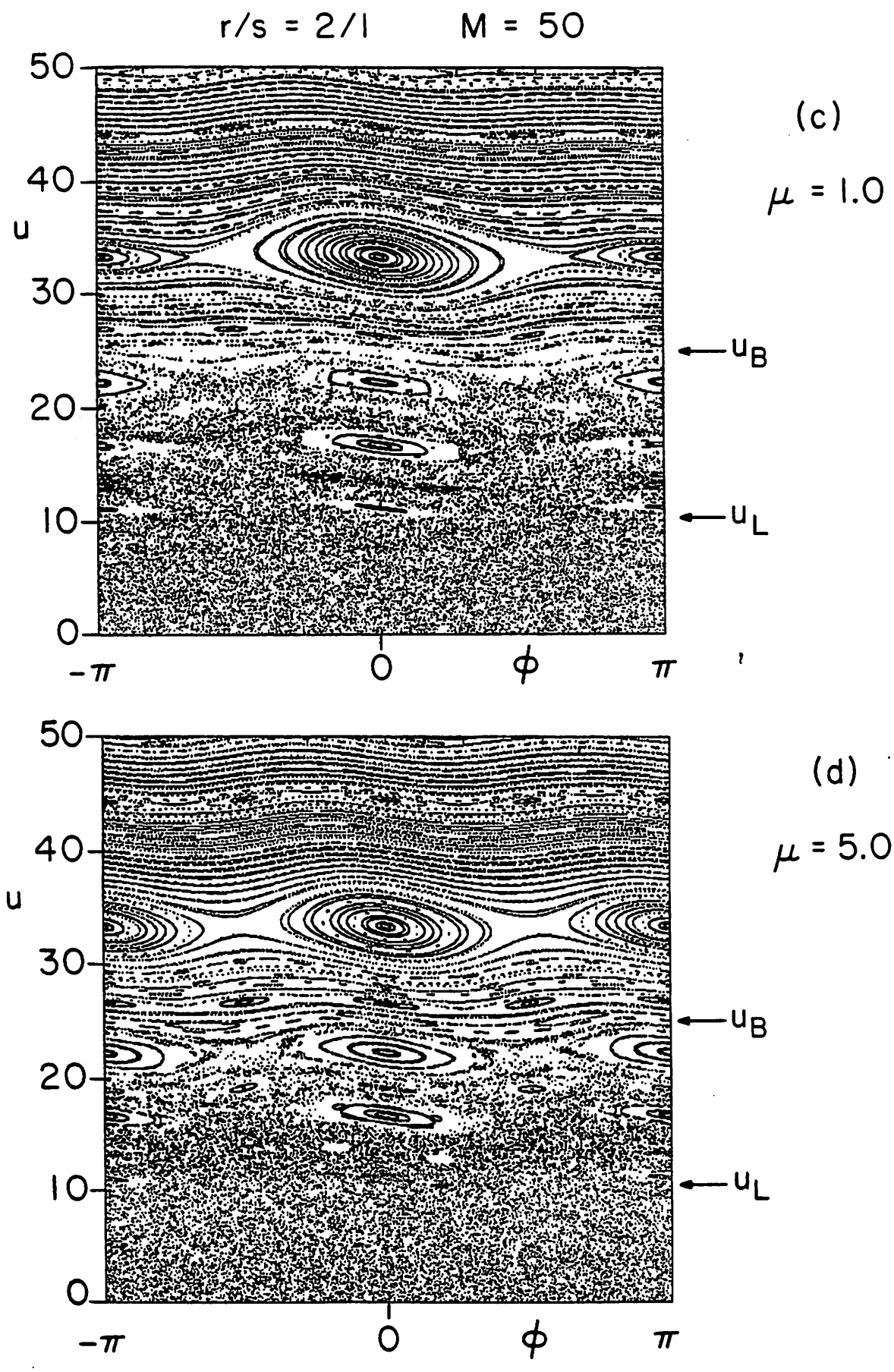
r/s = 2/1
M = 50
50
40
30
20
10
0
u
u_B
u_L
$-\pi$
0
ϕ
π
(c)
μ = 1.0
(d)
μ = 5.0

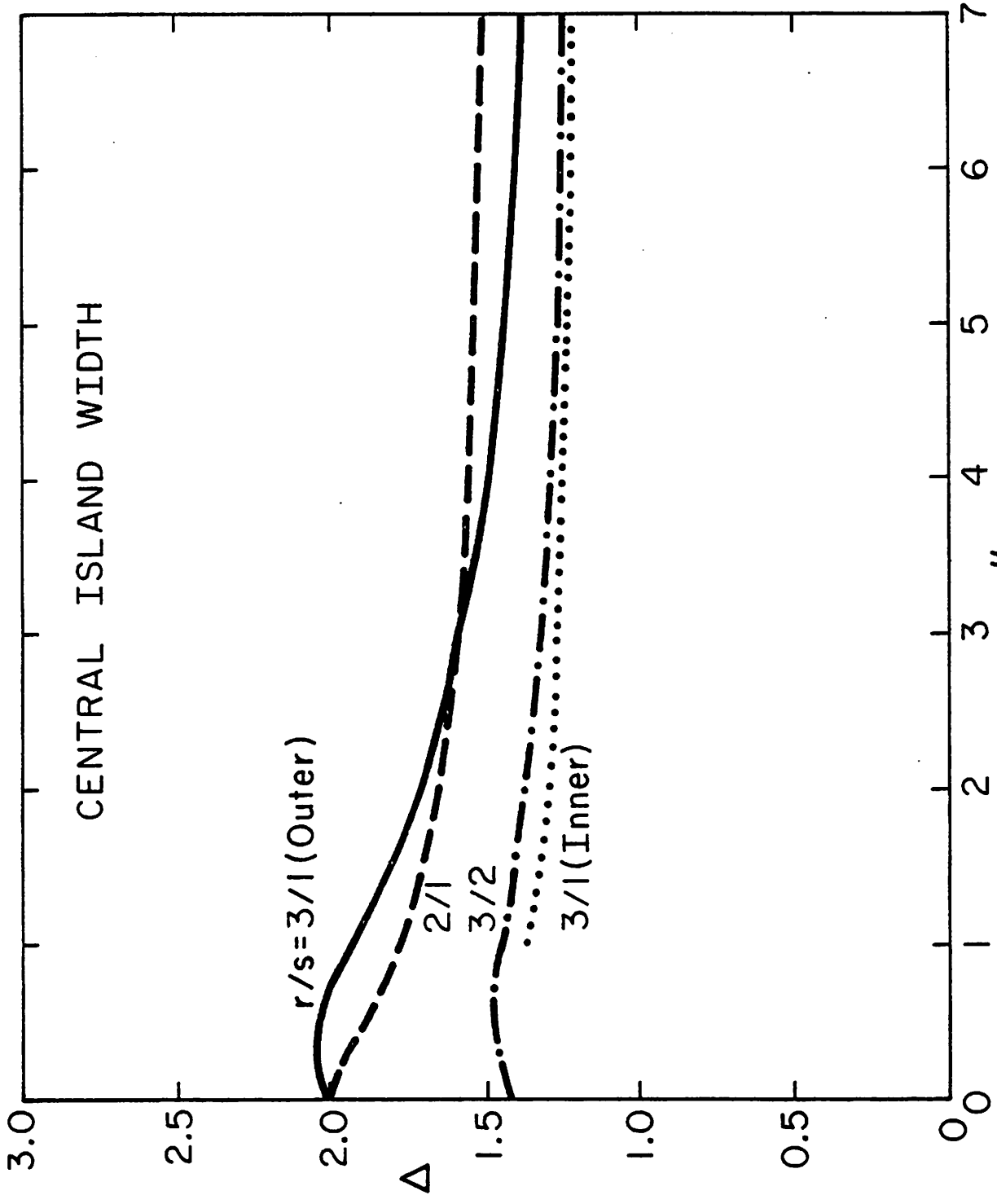

Fig. 5. Island width vs. amplitude ratio for r/s = 2/1, 3/2 and 3/1 (inner separatrix does not exist for $\mu < 1$).

the variation in Δ is only about 10%, so that we may safely take $\Delta(\mu) \approx \Delta(0)$ in deriving overlap criteria.

4.2 $\boxed{r/s = 3/2}$.

Since $r - s = 1$, we again have the immediate complete solution that the $\phi_0 = \pi$ fixed point bifurcates at $\mu^* = 2/3$, while the $\phi_0 = 0$ elliptic fixed point stays put. Formally, Eq. (15) becomes

$$4x^2 + \frac{2}{\mu} x - 1 = 0, \tag{19}$$

whose solutions are

$$4\mu\cos\phi_0 = -1 \pm \sqrt{1+4\mu^2}. \tag{20}$$

While (20) has no double roots, there is a double root in ϕ_0 when $\cos\phi_0 = -1$, where $\cos\phi_0$ is locally quadratic near $\phi_0 = \pi$. The second root of (20) locates the nonbifurcating hyperbolic fixed points. At $\phi_0 = \pi$, $V' = V'' = V''' = 0$ and $V^{iv} > 0$, indicating a pitchfork bifurcation. Figure 6 shows a series of level curves and effective potentials, this time over two complete cycles, in order to better illustrate the figure eight inner separatrix that develops at $\phi_0 = \pi$ when $\mu > \mu^*$ These plots are to be compared with the exact mappings in Ref. 1. Note that in all cases the island width is greatest at $\phi_0 = 0$, so that the central islands are expected to overlap first.

We now turn to the calculation of the island width for this paradigm case. From (20), the crossing phase ($u = 0$) is given by

$$4\mu \cos\phi_c = \sqrt{1+4\mu^2} - 1. \tag{21}$$

Using (21) in (11) then gives

$$12\mu^2\sqrt{1+\mu^2}\, G\Delta^2 = 8\mu^3 + 18\mu^2 - 1 + (1+4\mu^2)^{3/2} \tag{22}$$

which holds for all μ. As Fig. 5 shows, the width is quite flat in this case, having a gentle maximum at $\mu \approx 0.5$ after which it decreases

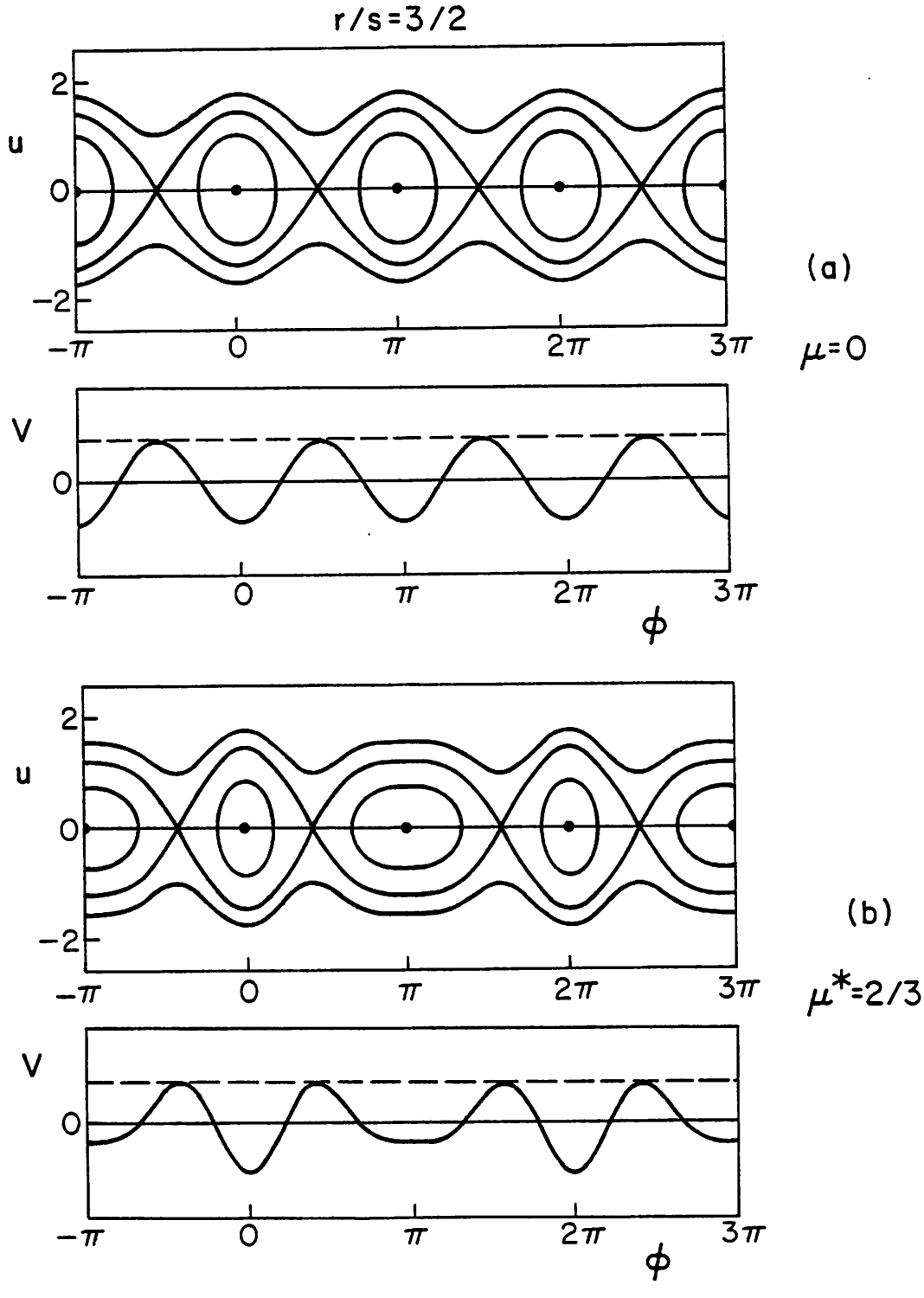

Fig. 6. Level curves and effective potential for r/s = 3/2. A pitchfork bifurcation occurs at $\phi = \pi$ when $\mu = 2/3$.

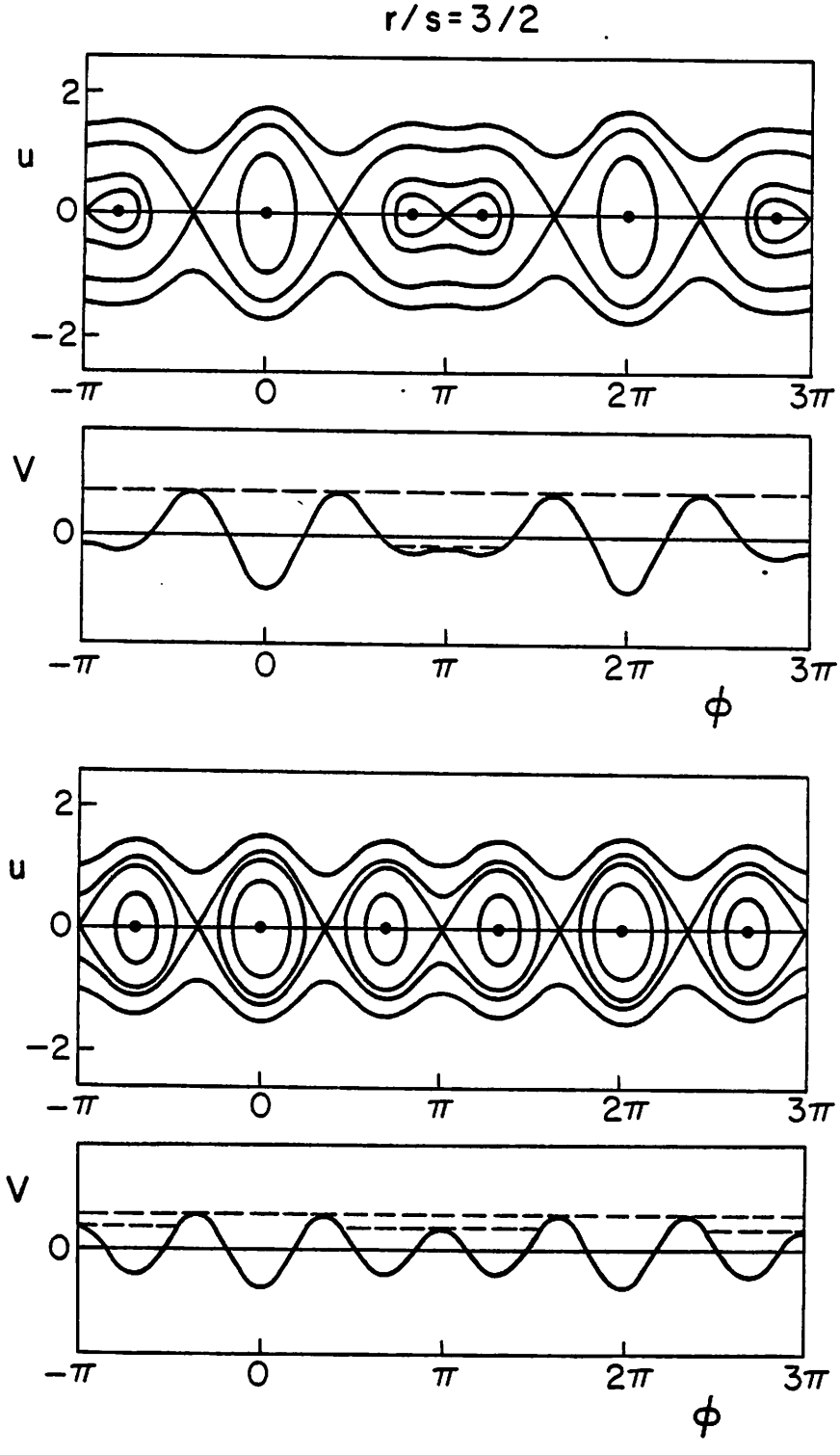
r/s=3/2
u
V
2
0
-2
-π
π
2π
3π
φ
(c)
μ=1
(d)
μ=5

monotonically to $\Delta(\infty) \approx 0.8\ \Delta(0)$. For this case $\Delta(\mu) \approx \Delta(0)$ is a good approximation over the entire range of μ.

The cases $r/s = 4/3$ and $5/4$ have the property $r = s + 1$ and yield mappings similar to the cases $r/s = 2/1$ and $3/2$.

4.3 $\boxed{r/s = 3/1}$

Since $r - s = 2$, it follows that tangent bifurcations occur at $\phi_0^* = 0$ and π but do not bifurcate for positive μ. Formally, (15) becomes

$$\cos^2\phi_0 = \frac{1}{4}\left(1 - \frac{1}{\mu}\right), \tag{23}$$

whose discriminant vanishes at $\mu = 1$. When $\mu > 1$, the crossing phase nearest $\phi_0 = 0$ is given by

$$\cos\phi_c = \frac{1}{2}\sqrt{1 - \frac{1}{\mu}}\ . \tag{24}$$

As Fig. 7 shows, there is a single separatrix for $\mu < 1$ and nested inner and outer separatrices for $\mu \geq 1$. The width of the outer separatrix is given by

$$G\Delta^2_{outer} = \frac{4(1+\mu/3)}{\sqrt{1+\mu^2}}\ , \tag{25}$$

while, using (24), we find for the inner width,

$$3\sqrt{1+\mu^2}\ G\Delta^2_{inner} = 2(3+\mu) + 2(\mu-1)\sqrt{1 - \frac{1}{4\mu}}\ . \tag{26}$$

The variation of the two widths with μ is shown in Fig. 5. While Δ_{outer} is obviously the relevant width to use in an overlap criterion, Δ_{inner} can play a subtle role. For, as both separatrices are adorned with their own stochastic layers, the intriguing possibility of self-overlap arises, in which the two stochastic layers strongly interact, destroying all KAM curves in their vincinity. In fact, as can be seen from the curves in Fig. 5, the two separatrices eventually

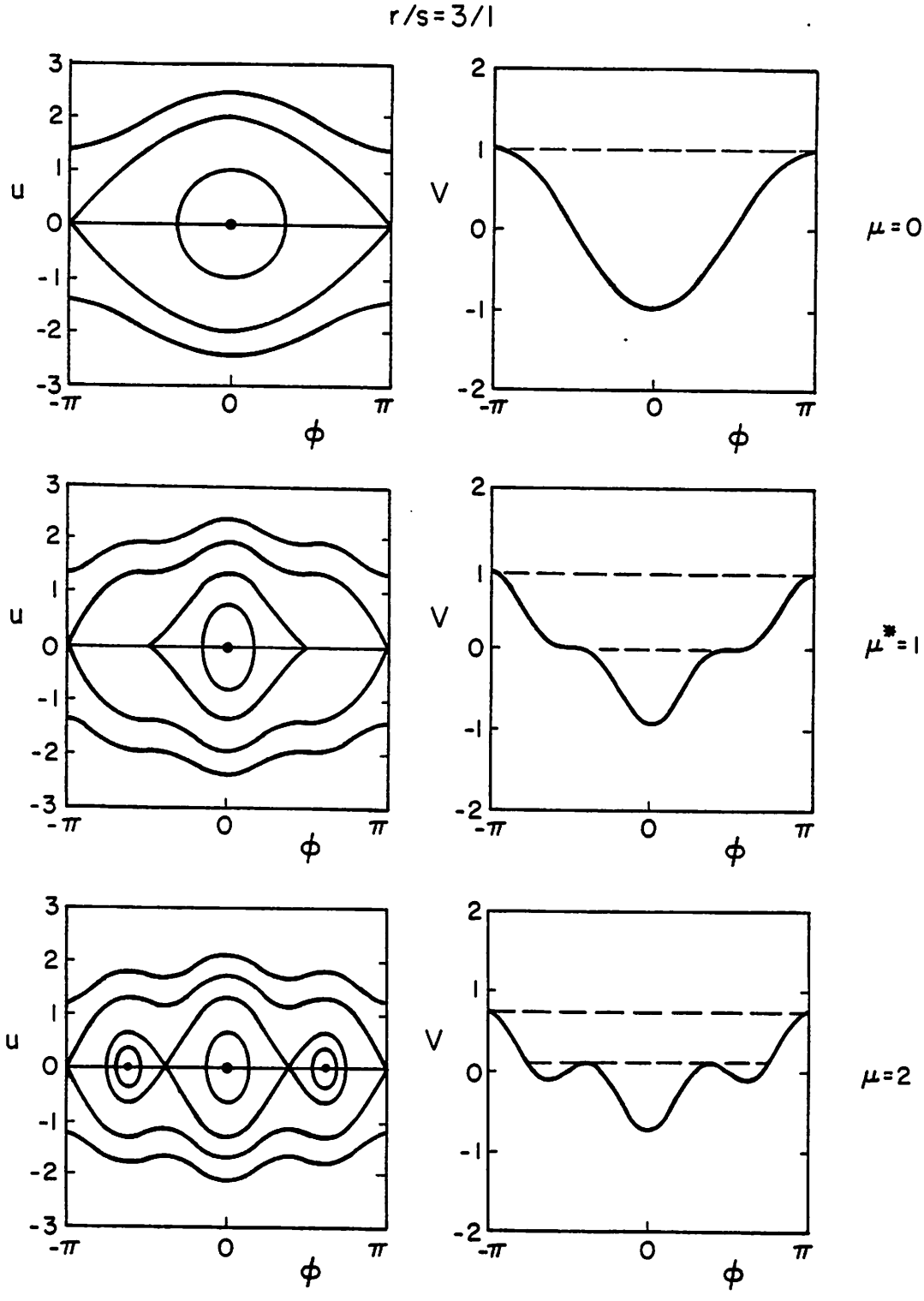

Fig. 7. Level curves and effective potential for r/s = 3/1. Tangent bifurcations take place at at $\phi = \pm\pi/2$ when $\mu = 1$.

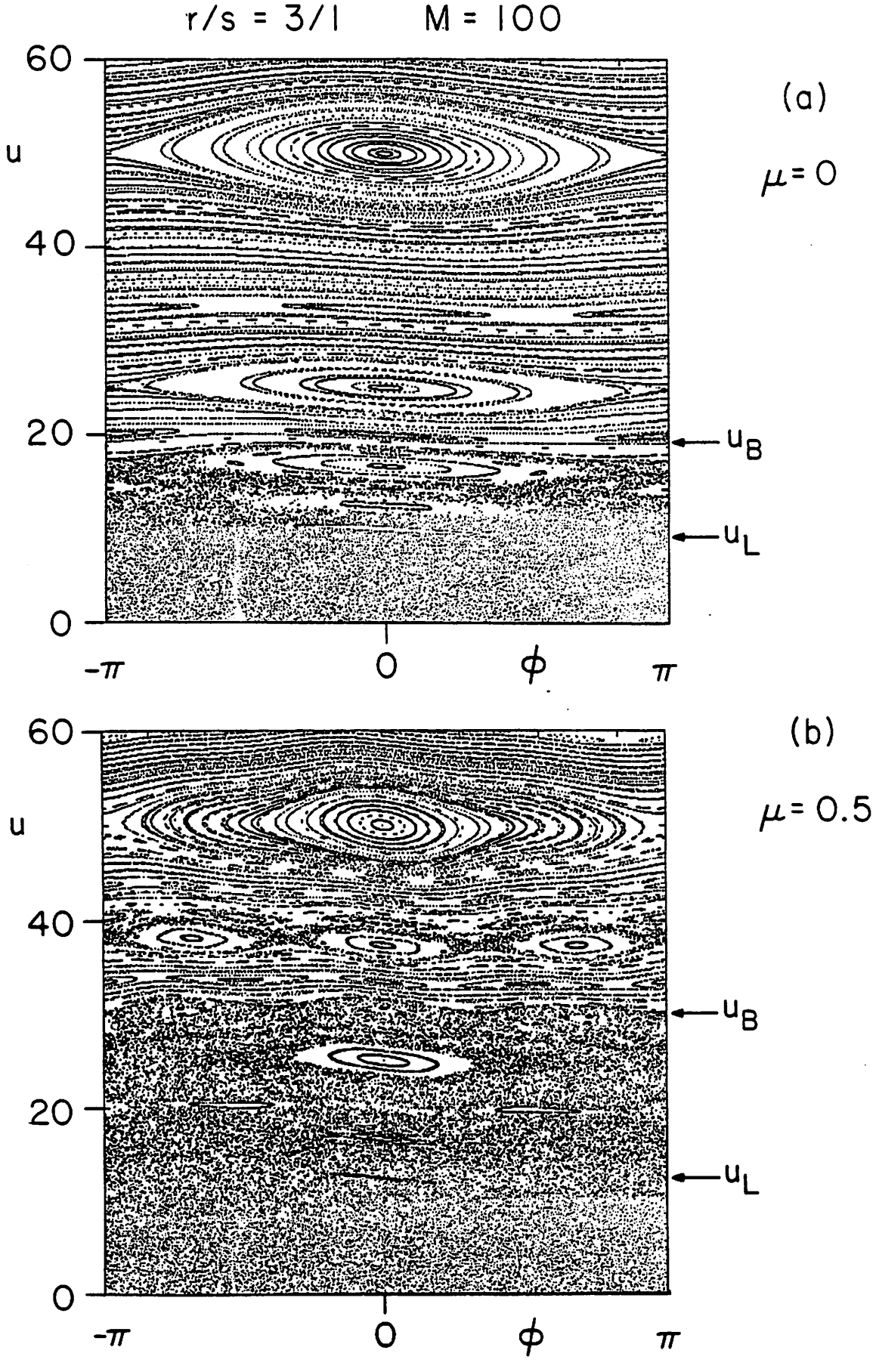

Fig. 8. Numerical mappings for r/s = 3/1, M = 100. Note bifurcation of common islands at u = 50 and 25.

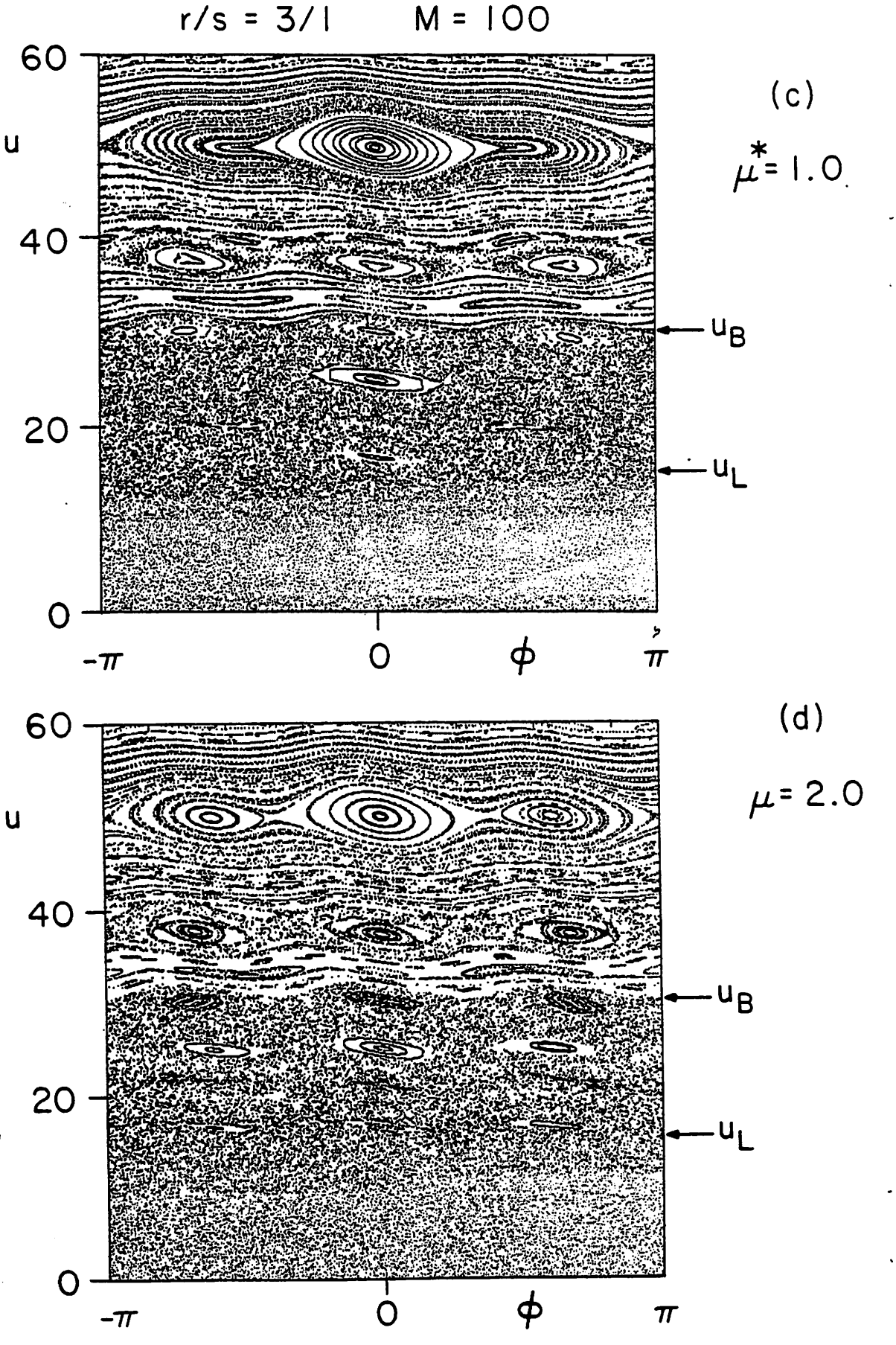
r/s = 3/1 M = 100
60
40
20
0
u
u_B
u_L
$-\pi$
0
ϕ
π
(c)
$\mu^* = 1.0$
(d)
$\mu = 2.0$

merge as $\mu \to \infty$. Consequently, in parameter ranges where islands are nearly overlapping, such complex nested structures may dissolve rather rapidly. This tendency is apparent in the set of mappings shown in Fig. 8.

We also note in passing that the inner separatrix at bifurcation ($\mu = 1$) has the simple form

$$Gu^2 = \frac{4}{3}\sqrt{2}\cos^3\phi, \quad |\phi| \leq \pi/2. \tag{27}$$

4.4 r/s = 4/1

To determine the bifurcation sequence we write (15) as

$$8x^3 - 4x + \frac{1}{\mu} = 0. \tag{28}$$

Rather than work out the discriminant for this cubic, we instead write out (13),

$$8x^4 - 8x^2 + \frac{1}{4\mu}x + 1 = 0. \tag{29}$$

Equations (28) and (29) then combine to give

$$6x^4 - 7x^2 + 1 = 0, \tag{30}$$

a quadratic in x^2. The real roots for $\mu > 0$ are

$$\begin{aligned} \cos\phi_0^* &= -1 \qquad \mu^* = \frac{1}{4} \\ \cos\phi_0^* &= \frac{1}{\sqrt{6}} \qquad \mu^* = \frac{3}{8}\sqrt{6} = 0.9186 \end{aligned} \tag{31}$$

Thus, the metamorphosis from one to four-fold symmetry proceeds in two stages; when $\mu = 1/4$ there is an anti-pitchfork bifurcation at $\phi_0 = 180°$, followed by tangent bifurcations at $\phi_0 = \pm 65.91°$ when $\mu = 0.9186$. In order to calculate level curves including the inner and outer separatrices, a complete solution of (28) is required to give $\phi_c(\mu)$. While this is straightforward, for the sake of brevity

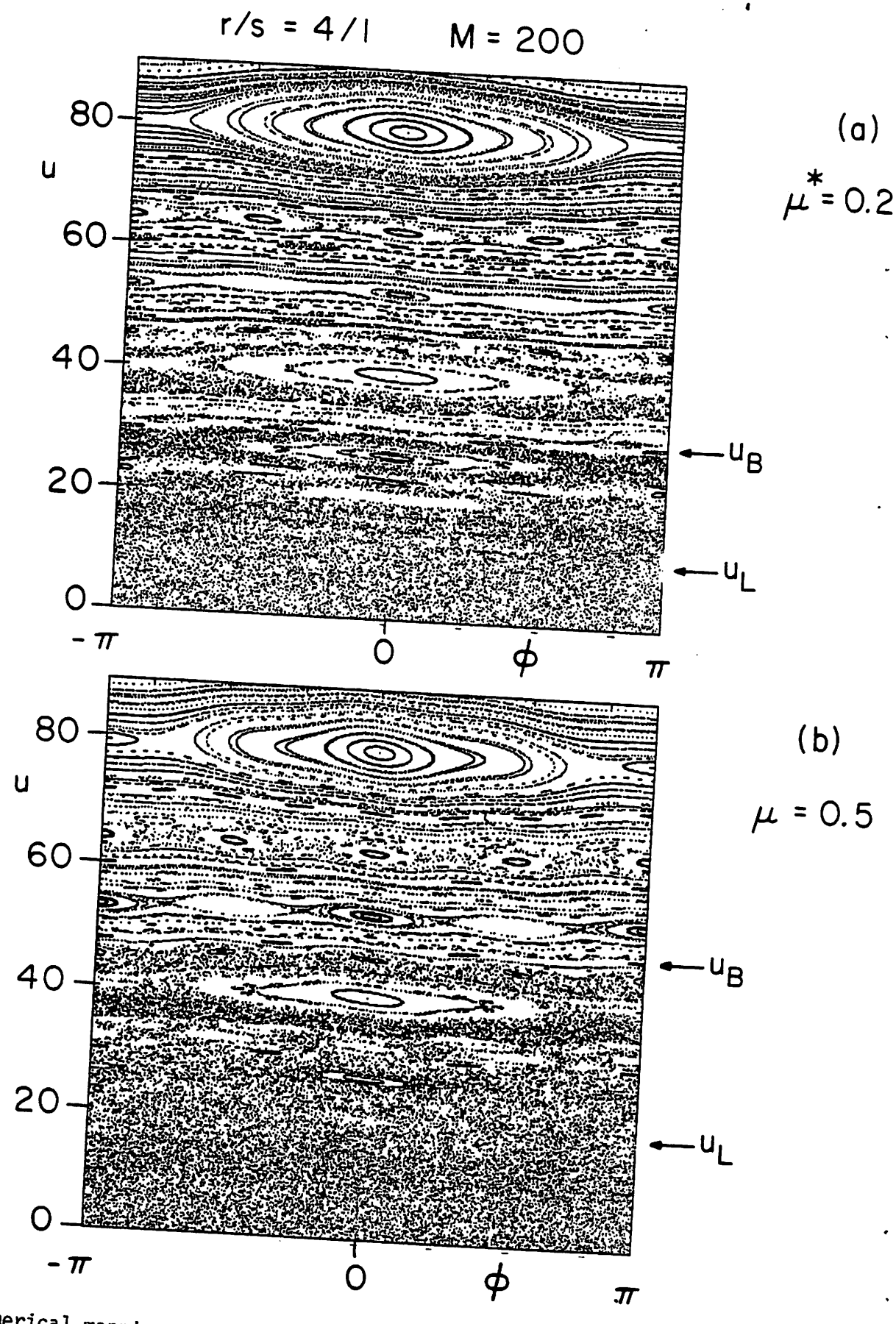

Fig. 9. Numerical mappings for r/s = 4/1 and M = 200. An anti-pitchfork bifurcation occurs at $\phi = \pi$ when $\mu = 0.25$, followed by tangent bifurcations at $\phi = \pm 65.91°$ when $\mu = 0.9186$.

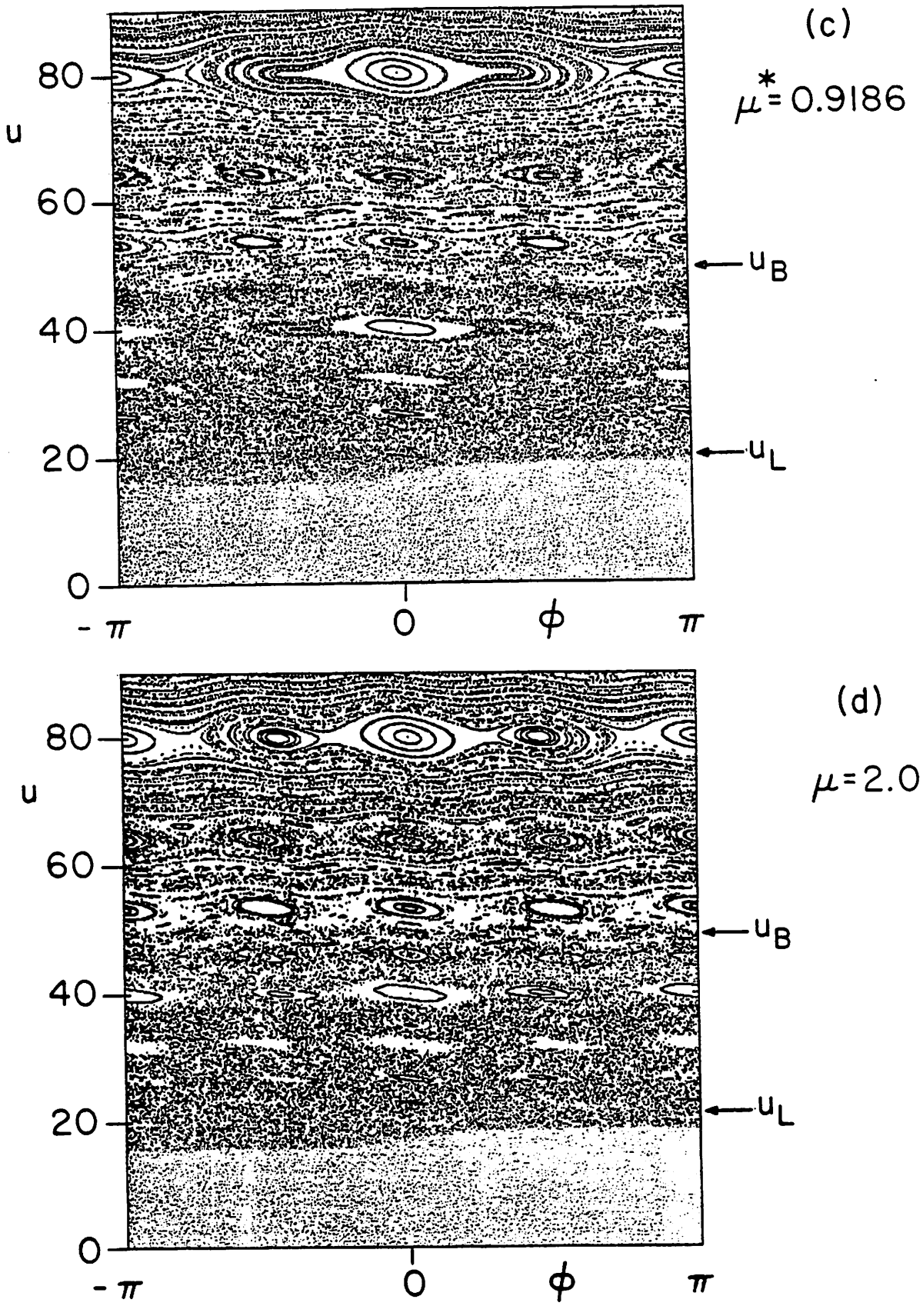
r/s = 4/1 M = 200
(c)
$\mu^* = 0.9186$
u
80
60
40
20
0
u_B
u_L
$-\pi$
0
ϕ
π
(d)
$\mu = 2.0$
u
80
60
40
20
0
u_B
u_L
$-\pi$
0
ϕ
π

we include (Fig. 9) only the numerical mappings, which show not only the bifurcations but also the development of a thick stochastic layer about the inner separatrix near the cusp of the tangent bifurcation. Note that even though the central island width shrinks by a factor of two as μ increases from 0 to ∞, there is still a substantial increase in the adiabatic barrier, from $u_b = 22$ to $u_b \approx 48$. This is because the enhanced stochasticity is due primarily to the growth of the r-fold islands, producing overlap at fairly low μ, before the common islands have shrunk appreciably. In such cases where closed form expressions for $\Delta(\mu)$ are difficult or impossible to obtain, we therefore employ the limiting form $\Delta(0)$ given by (11). In modelling ECRH where closely spaced frequencies are called for, we naturally take $r \approx s$, in which case the variation in $\Delta(\mu)$ is entirely negligible.

4.5 $\boxed{r/s = 5/1}$

The polynomial (15) becomes

$$16x^4 - 12x^2 + (1 + \frac{1}{\mu}) = 0 \tag{32}$$

which is simply a quadratic in x^2. The solution is

$$8x^2 = 3 \pm \sqrt{5-4/\mu} \ . \tag{33}$$

A pair of double roots evidently occurs for

$$\mu^* = 4/5 \tag{34}$$

at angles given by

$$\cos\phi_0^* = \pm \sqrt{3/8} \tag{35}$$

or

$$\phi_0^* = \pm 52.24°, \pm 127.76°.$$

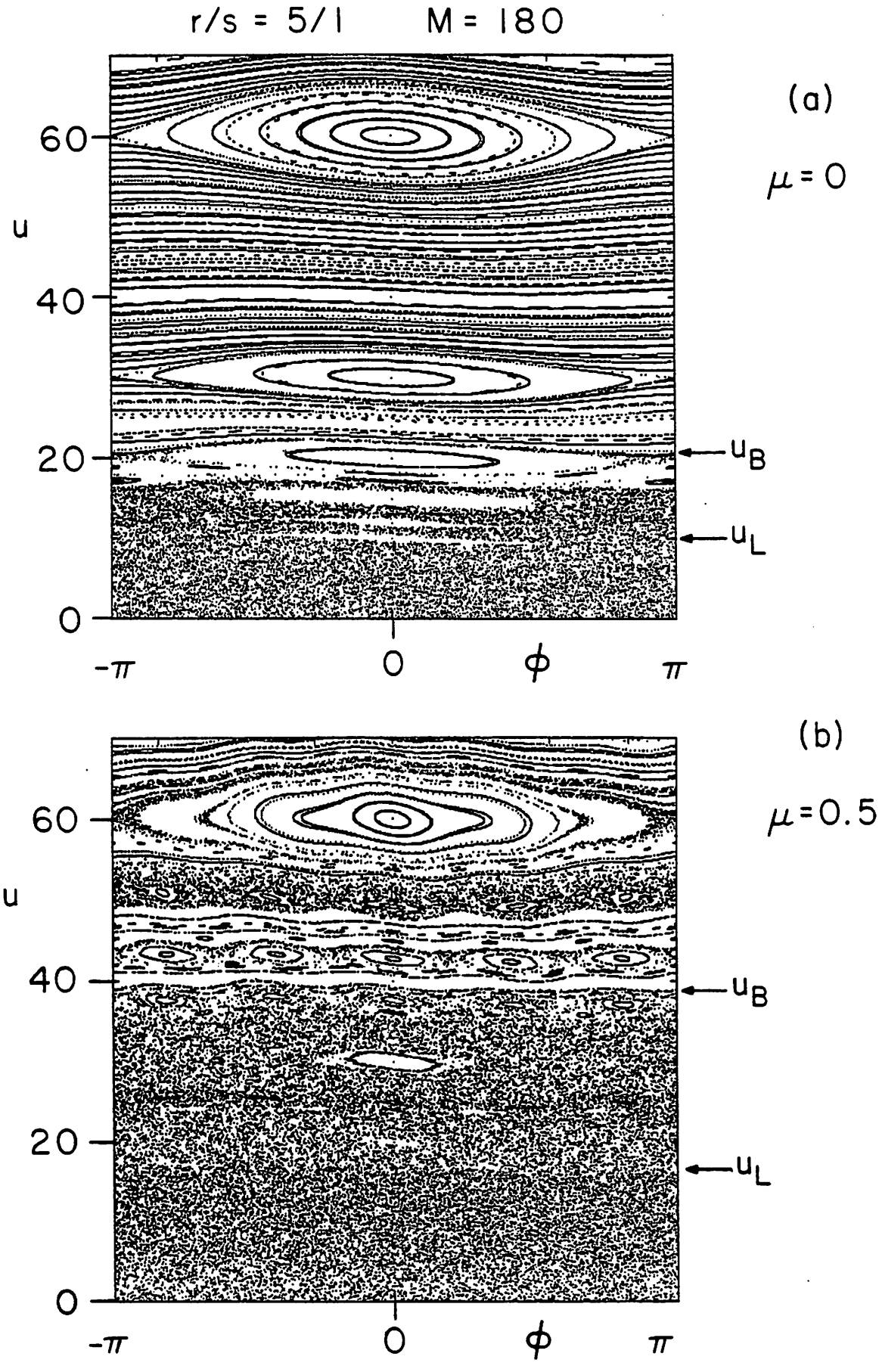

Fig. 10. Numerical mappings for r/s = 5/1 and M = 180. A spectacular double-tangent bifurcation occurs at $\phi = \pm 52.24°$ and 127.76° when $\mu = 4/5$. Note the existence of narrow adiabatic bands sandwiched between broad stochastic layers, especially at $\mu = 2.0$.

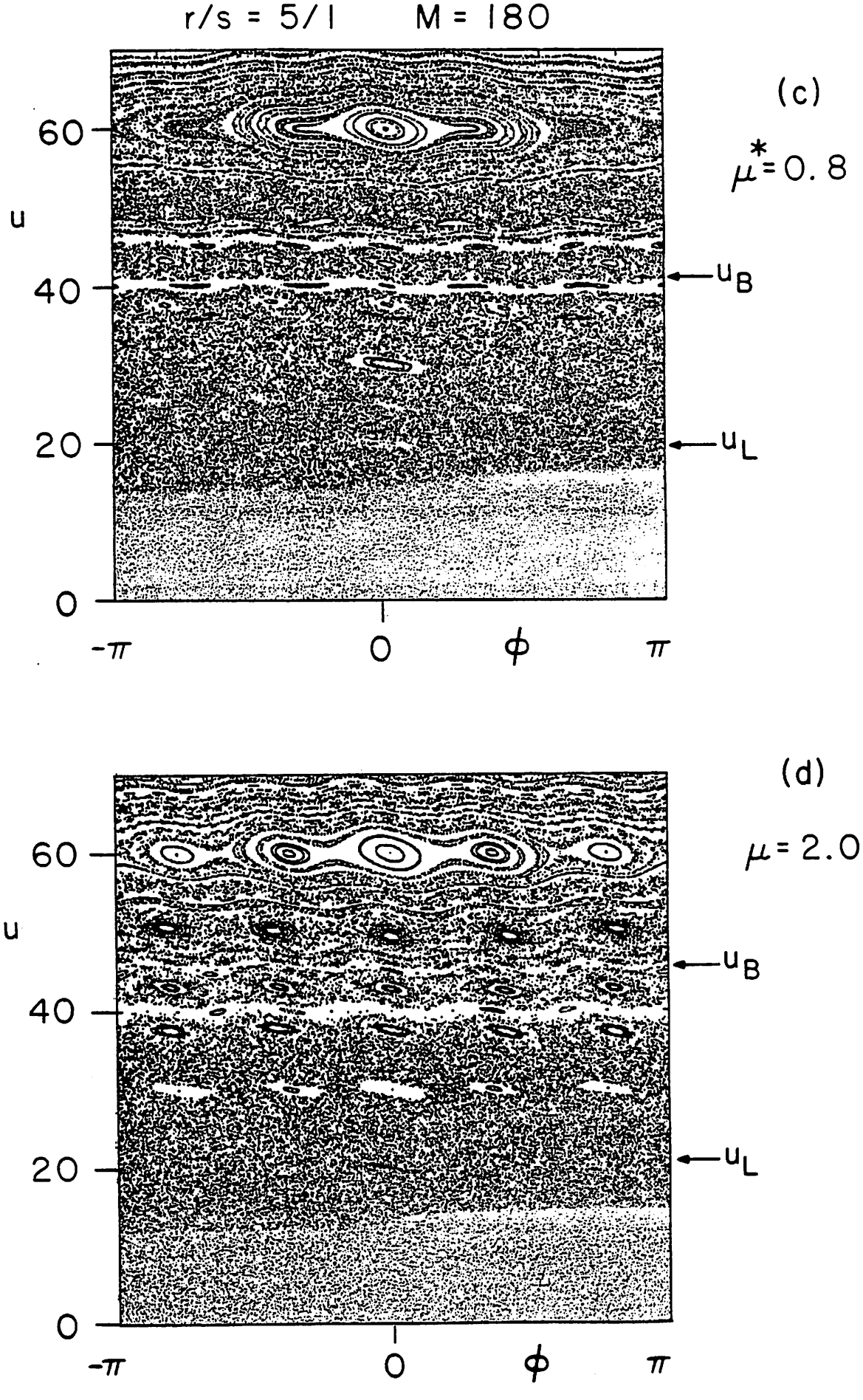
r/s = 5/1 M = 180
(c)
$\mu^* = 0.8$
u
60
40
20
0
u_B
u_L
$-\pi$
0
ϕ
π
(d)
$\mu = 2.0$
u
60
40
20
0
u_B
u_L
$-\pi$
0
ϕ
π

Thus, we have the unusual coincidence of two simultaneous nested tangent bifurcations at a single value of μ, arranged as shown in Fig. 10. There are actually three nested separatrices in Fig. 10d!

4.6 $\boxed{r/s = 5/3}$

The polynomial (15) becomes

$$16\mu x^4 + 4(1-3\mu)x^2 + \mu - 1 = 0 \tag{36}$$

with solution

$$8\mu x^2 = 3\mu - 1 \pm \sqrt{5\mu^2 - 2\mu + 1}\,. \tag{37}$$

In this case the double root occurs for $x^2 = 0$, as the discriminant of (37) never vanishes for positive μ. Of course, since $r = s + 2$ we knew a priori that tangent bifurcations occur at $\phi_0^* = \pm\pi/2$, when $\mu^* = 1$. A set of mappings is presented in Fig. 11, which reveals a very interesting pair of one-sided tangent bifurcations.

4.7 $\boxed{r/s = 5/2}$

Finally we come to the last, and most challenging, of the tractable bifurcations. The polynomial (15) to be solved is

$$x^4 - \frac{3}{4}x^3 + \frac{1}{8\mu}x + \frac{1}{16} = 0\,. \tag{38}$$

Since r-s is odd, we know that bifurcations occur for $\mu_1^* = 2/5$ at $\phi_0^* = \pm\pi$. The other (tangent) bifurcations take place at a μ where (38) has a double root.

From the classical theory of equations [8], the discriminant Δ_4 of (38) is equal to the discriminant Δ_3 of its "resolvant cubic,"

$$y^3 + \frac{1}{2}qy^2 + \frac{1}{16}(q^2-4s)y - \frac{1}{16}r^2 = 0 \tag{39}$$

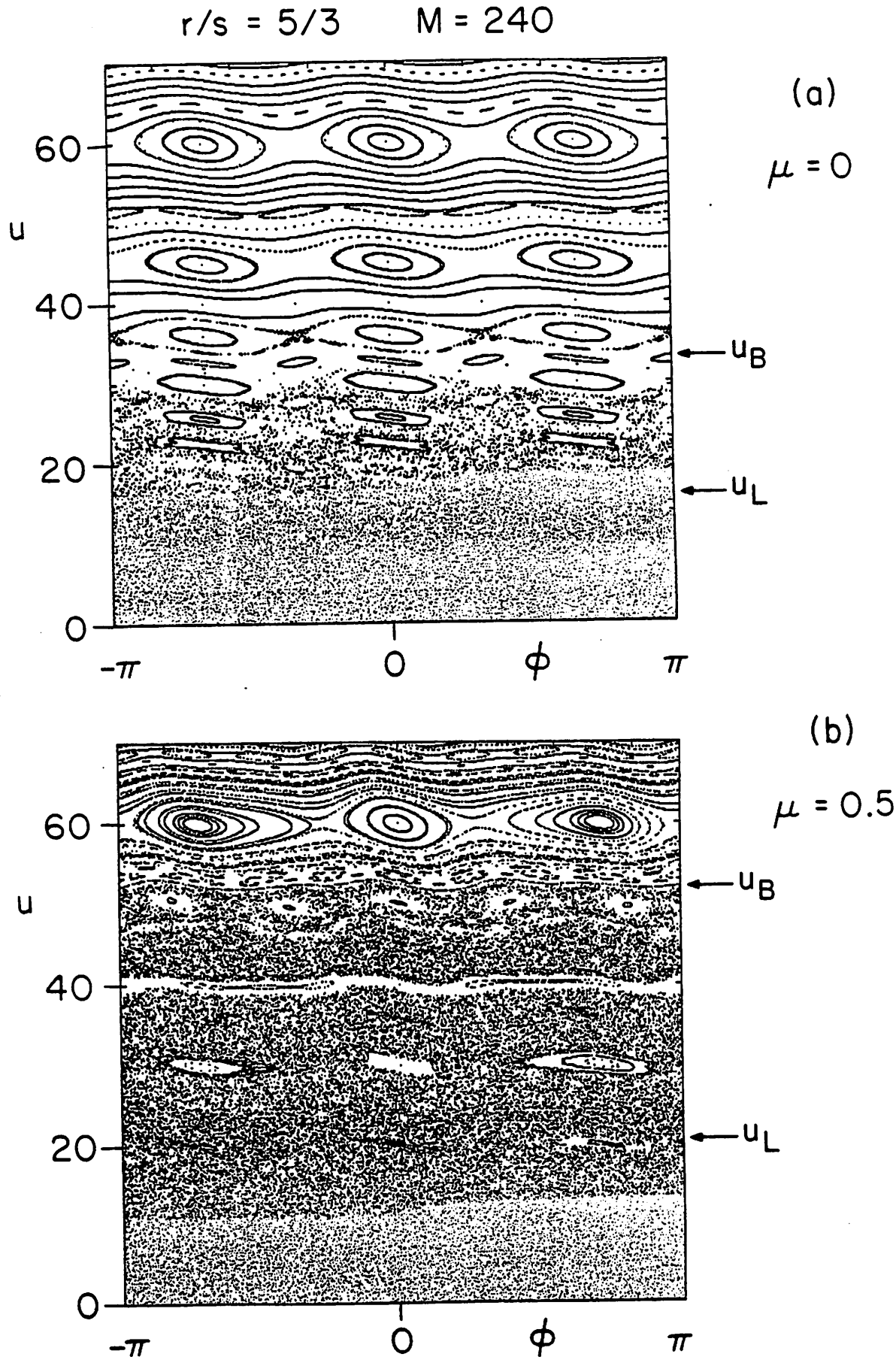

Fig. 11. Numerical mappings for r/s = 5/3 and M = 240. An interesting pair of one-sided tangent bifurcations occurs at $\phi = \pm\pi/2$ when $\mu = 1$.

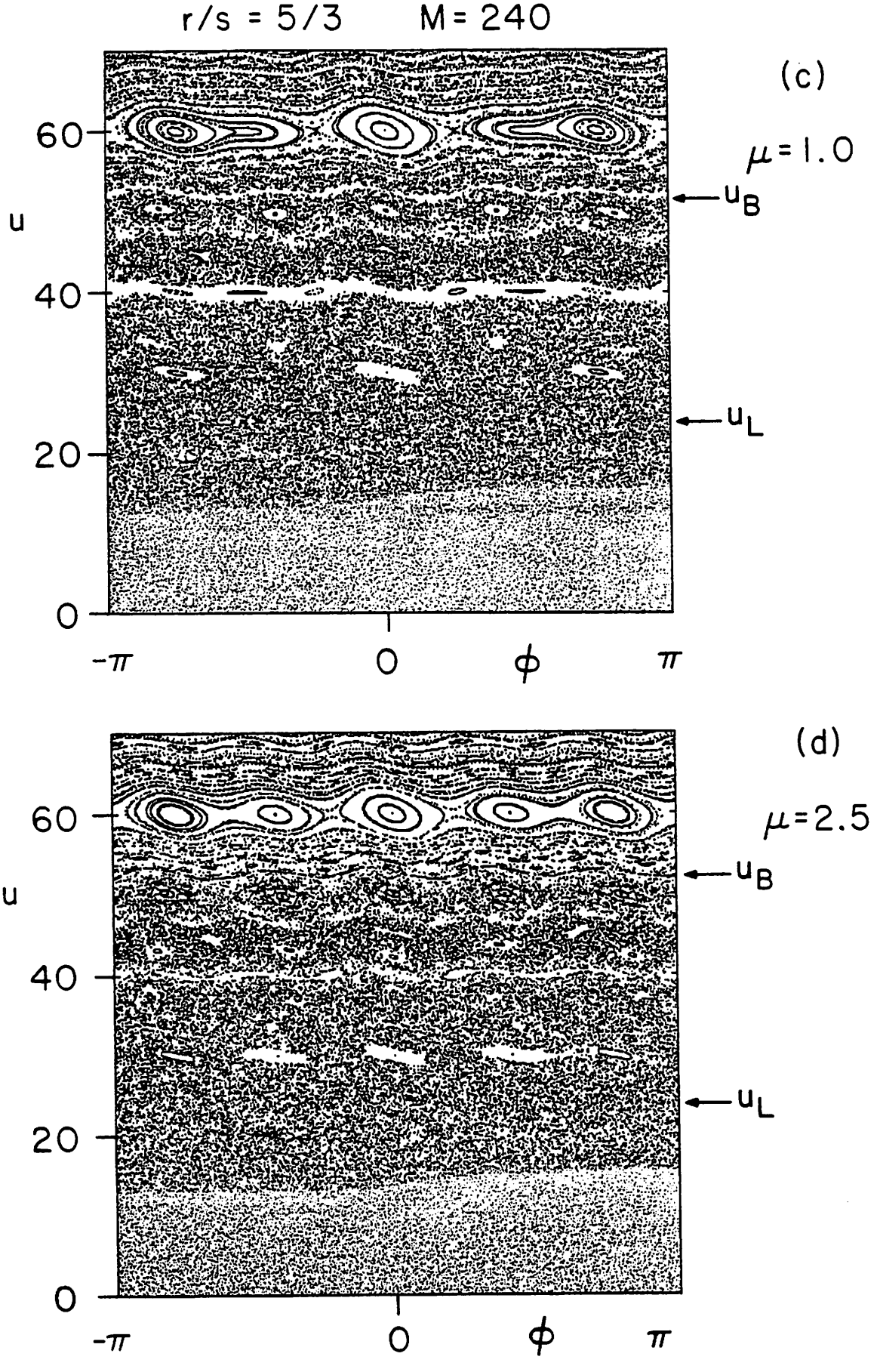
r/s = 5/3
M = 240
(c)
μ = 1.0
u_B
u_L
60
40
20
0
u
-π
0
φ
π
(d)
μ = 2.5
u_B
u_L
60
40
20
0
u
-π
0
φ
π

where

$$q = -\frac{3}{4},\ r = \frac{1}{8\mu},\ s = \frac{1}{16}\ .$$

Here, r and s are not to be confused with our original frequency ratio. To find Δ_3, we transform (39) to the reduced cubic

$$Y^3 + PY + Q = 0, \tag{40}$$

with

$$P = C - \frac{1}{3}B^2$$

$$Q = D - \frac{1}{3}BC + \frac{2}{27}B^3,$$

where, from (39),

$$B = \frac{1}{2}q = -\frac{3}{8}$$

$$C = \frac{1}{16}(q^2-4s) = \frac{5}{256}$$

$$D = -\frac{1}{16}r^2 = -\frac{1}{(64\mu)^2}\ .$$

For a double root,

$$\Delta_3 = \frac{1}{27}P^3 + \frac{1}{4}Q^2 = 0$$

which gives

$$\mu_2^* = \left(\frac{14}{9}\sqrt{21} - 6\right)^{-1/2} = 0.94137. \tag{41}$$

The corresponding value of ϕ_0^* is best found by solving eq. (6) iteratively, rather than suffering through the formal solution of (38). The result is

$$\phi_0^* = 55.80°. \tag{42}$$

The sequence of bifurcations is illustrated in the set of computer-produced mappings in Fig. 12.

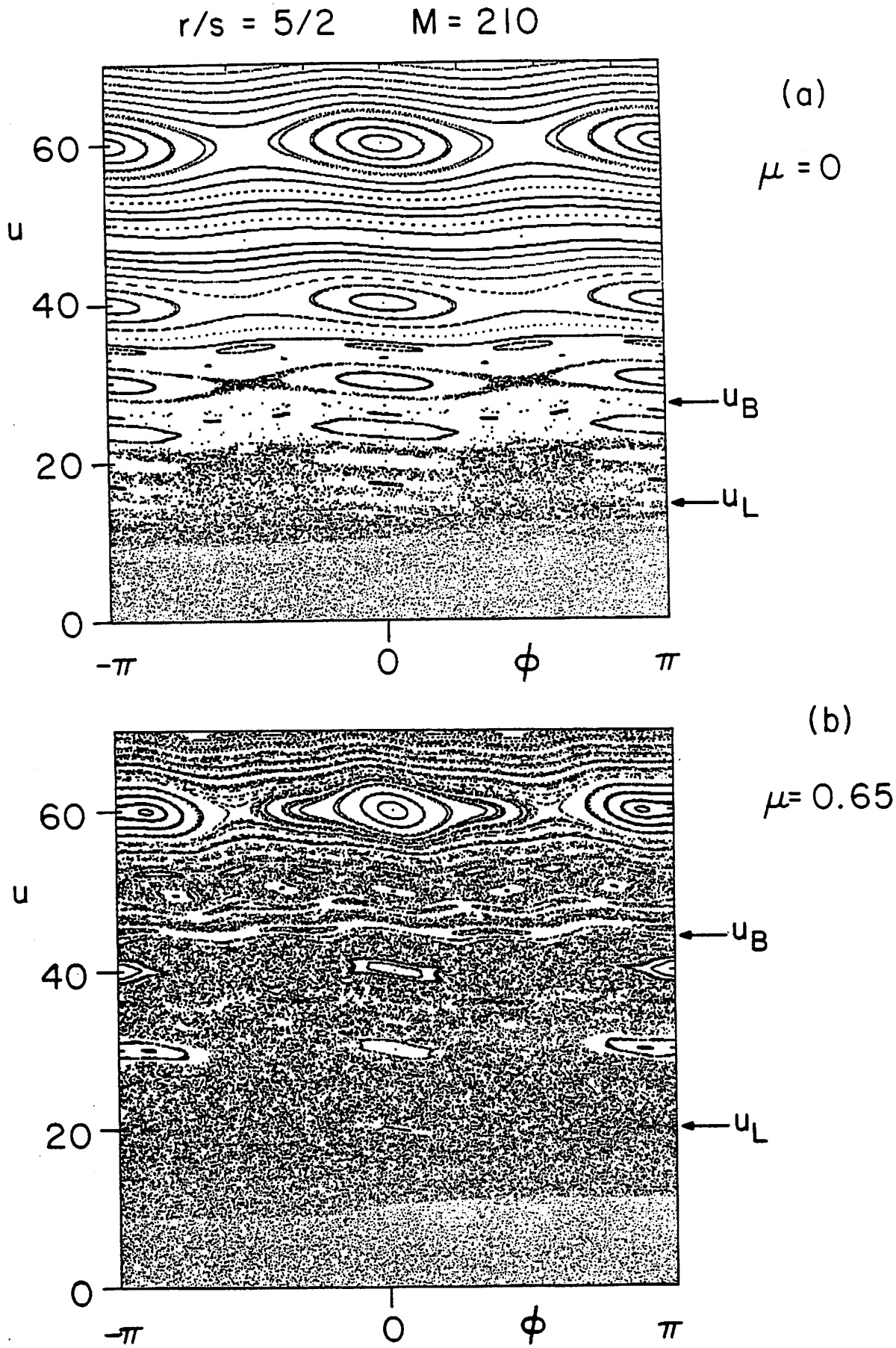

Fig. 12. Numerical mappings for r/s = 5/2 and M = 210. An anti-pitchfork bifurcation occurs at $\phi = \pi$ when $\mu = 2/5$, followed by tangent bifurcations at $\phi = 55.80°$ when $\mu = 0.9414$.

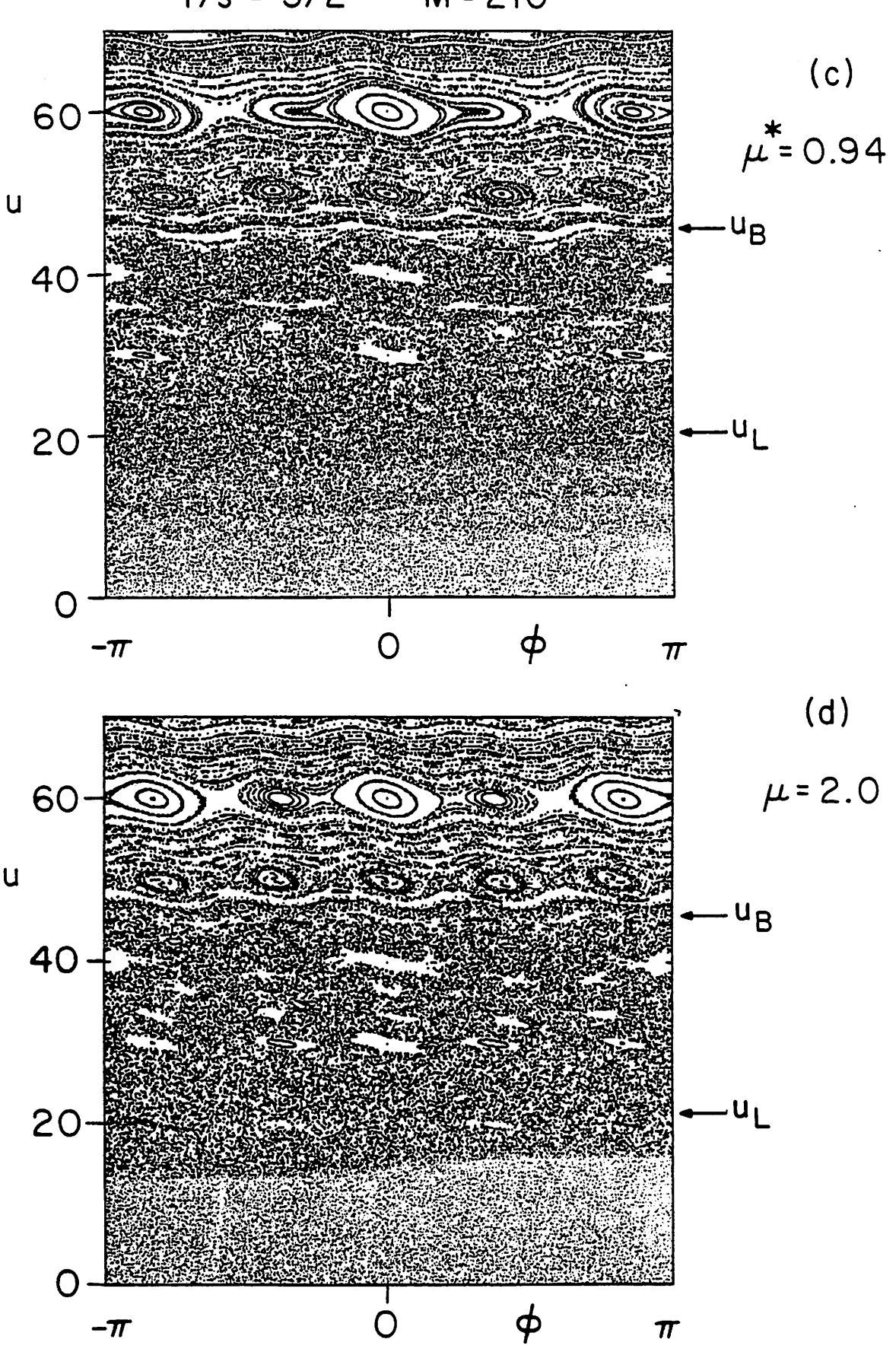
r/s = 5/2 M = 210
(c)
$\mu^* = 0.94$
60
40
20
0
u
u_B
u_L
$-\pi$
0
ϕ
π
(d)
$\mu = 2.0$
60
40
20
0
u
u_B
u_L
$-\pi$
0
ϕ
π

5. Discussion

We have explored in some detail the manner in which the island width depends on the changing topology of the two-frequency Fermi map, as the relative strength of the two components is varied. A well-defined island width appropriate to an overlap criterion was derived and applied to three paradigm cases. The results show that in most instances the width of the common islands is well approximated by $\Delta(0)$, with no r-component present.

The bifurcations suffered by the common islands as the mapping changes from s-fold to r-fold symmetry were shown to be particular examples of a general family of bifurcations occurring in one-dimensional periodic Hamiltonian systems with a variable parameter. These bifurcations were classified and related to the critical points of the periodic potential. Closed-form solutions of the bifurcation equations were then obtained for some particular values of r/s for the Fermi mapping. The calculated bifurcation thresholds were found to be in excellent agreement with computer-produced mappings.

In the above-mentioned cases, the fixed points move horizontally along lines of constant u and may be appropriately termed one-dimensional bifurcations. However, it is well known that more complex, two-dimensional bifurcations can occur. For example, as M is varied in the single frequency Fermi mapping, families of three, four or more fixed points may be emitted or absorbed by primary fixed points [9]. Two-dimensional bifurcations can also occur for the two-frequency Fermi mapping as μ is varied, and M_{eff} held fixed. An example is shown in Figs. 13-14 for the case r/s = 5/4, M = 225 and μ = 0.25. Here we have a dazzling showcase of three- and four-way bifurcations of both r-fold and common islands with varying μ. Clearly these complex divisions fall outside the scope of the simple theory presented in this report and offer a fruitful area for further analysis.

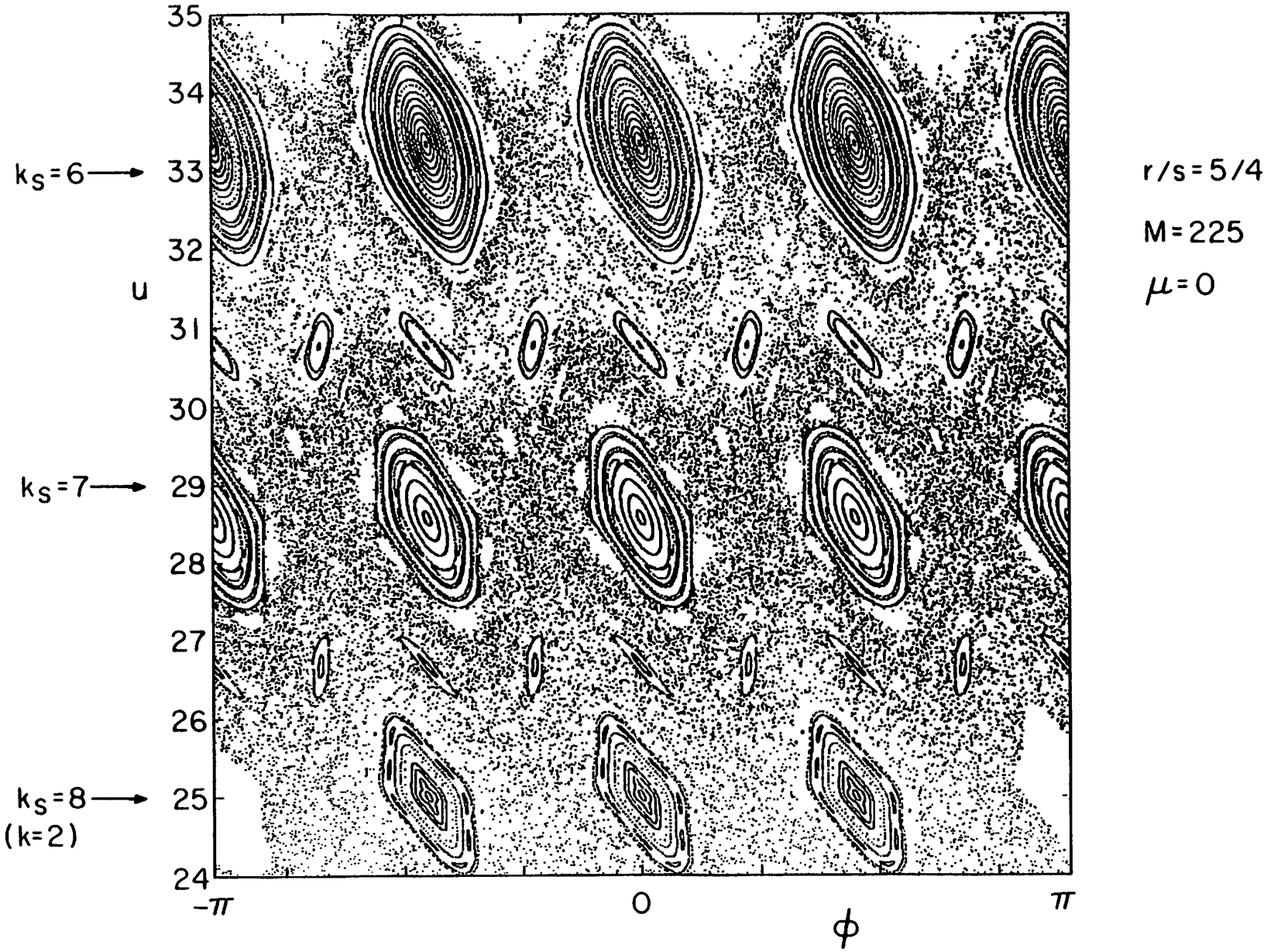

Fig. 13. Numerical mapping for r/s = 5/4, M = 225 and μ = 0. The island chains at u = 33.33 and u = 28.57 correspond to k_s = 6 and 7, while the islands at u = 25 are a k = 2 common chain.

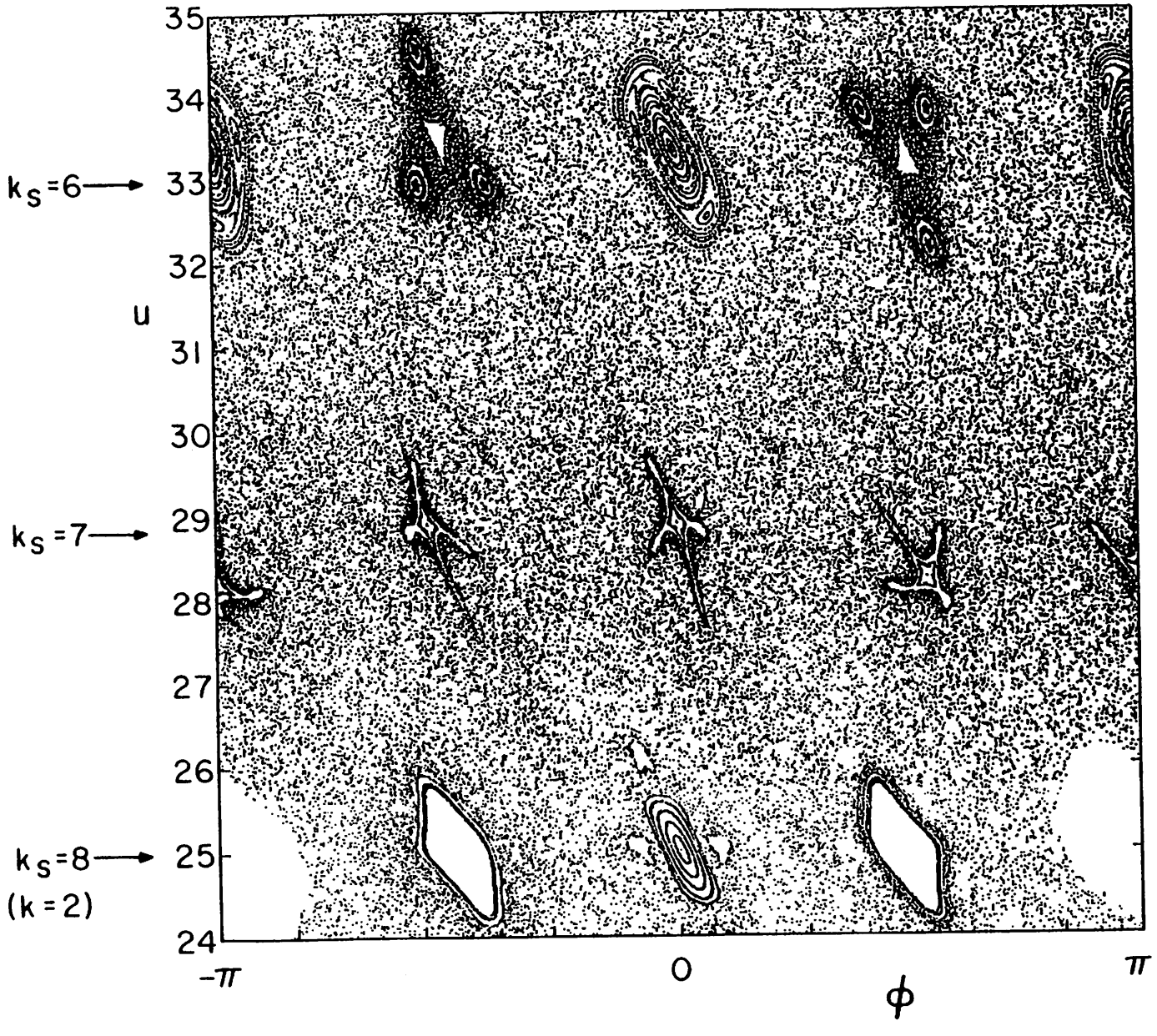

Fig. 14. Numerical mapping for r/s = 5/4, M = 225 and μ = 0.25. The k_s = 6 island at u = 33.33 and φ = 0 has emitted 3 islands, while its neighbors at φ = ±90° are absorbing 3 islands previously emitted at a smaller value of μ. The k_s = 7 islands near u = 29 are all undergoing four-way implosions. Note that the k_s islands are displaced vertically from their μ = 0 positions. The k = 2 common island at u = 25 and φ = 0 has undergone a (two dimensional) four-way bifurcation.

REFERENCES

[1] J. E. Howard, A. J. Lichtenberg and M. A. Lieberman, submitted to Physica D.

[2] G. M. Zaslavskii and B. V. Chirikov, Soviet Physics Doklady 9(1965) 989.

[3] M. A. Lieberman and A. J. Lichtenberg, Phys. Rev. A 5(1972) 1852.

[4] A. J. Lichtenberg, M. A. Lieberman and R. H. Cohen, Physica D 1(1980) 291.

[5] G. R. Smith, Lawrence Livermore Laboratory preprint UCRL-80121, Sept. 1977.

[6] T. Poston and I. Stewart, Catastrophe Theory and Its Applications (Pitman, London, 1978).

[7] I. Stewart, Physica D 2(1981) 245.

[8] L. E. Dickson, New First Course in the Theory of Equations (Wiley, New York, 1939) p 51.

[9] J. M. Greene, R. S. MacKay, F. Vivaldi and M. J. Feigenbaum, Princeton Plasma Physics Laboratory Report PPL-1745, Jan. 1981.